Research Network FWF S105

Photoacoustic Imaging in Medicine and Biology

http://pai.uibk.ac.at

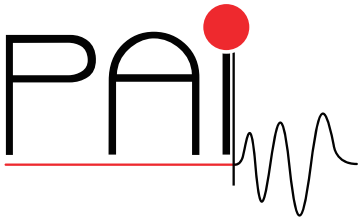

On a Decomposition Model for Optical Flow

J. Abhau, Z. Belhachmi,
and O. Scherzer

June 2009

PAI Report No. 15

FWF
Der Wissenschaftsfonds.

universität innsbruck

On a Decomposition Model for Optical Flow

J. Abhau[1], Z. Belhachmi[2], and O. Scherzer[3,4]

[1] Department of Mathematics, University of Innsbruck,
Technikerstrasse 21a, A-6020 Innsbruck, Austria,
Jochen.Abhau@uibk.ac.at
WWW home page: http://infmath.uibk.ac.at
[2] Laboratoire de Mathématiques LMAM, UMR 7122,
Université UPV-Metz, ISGMP,
Batiment A, Ile du Saulcy, 57045 Metz, France,
belhach@univ-metz.fr
[3] Department of Mathematics, University of Vienna,
Nordbergstrasse 15, A-1090 Wien, Austria
[4] Radon Institute of Computational and Applied Mathematics,
Altenberger Strasse 69, A-4040 Linz, Austria
otmar.scherzer@oeaw.ac.at

Abstract. In this paper we present a variational method for determining cartoon and texture components of the optical flow of a noisy image sequence. The method is realized by reformulating the optical flow problem first as a variational denoising problem for multi-channel data and then by applying decomposition methods. Thanks to the general formulation, several norms can be used for the decomposition. We study a decomposition for the optical flow into bounded variation and oscillating component in greater detail. Numerical examples demonstrate the capabilities of the proposed approach.

1 Introduction

Let be given $\Omega \subseteq \mathbb{R}^2$, a rectangular domain, and let the spatial-temporal function $f : \Omega \times [0, \infty) \to \mathbb{R}$ be a representation of a continuous image sequence. The goal of this work is to apply *image* decomposition methods to separate the optical flow belonging to f in texture and cartoon parts.

For this purpose we first review on optical flow estimation and decomposition methods.

Optical flow estimation.
Optical flow estimation is used to determine the motion in an image sequence by tracking pixels of constant intensity. For an excellent overview on optical flow estimation we refer to [11]. The standard optical flow model is differential and based on a Taylor series expansion, requiring that $f \in C^1(\Omega \times [0, \infty); \mathbb{R}^2)$. The optical flow is a characteristics $\boldsymbol{w} = (w_1, w_2)^T$, $w_1 = w_1(x_1, x_2, t)$, $w_2 = w_2(x_1, x_2, t)$ of the differential equation

$$f_t + f_{x_1} w_1 + f_{x_2} w_2 = 0 \text{ for } (x_1, x_2) \in \Omega, t \in [0, \infty) \, . \tag{1}$$

In mathematical terms *characteristics* are the paths of constant intensity. Variational optical flow methods are based on least squares formulations, consisting in minimization of the functional

$$\boldsymbol{w} \to \mathcal{S}(\boldsymbol{w}) := \frac{1}{2} \left\| f_t + f_{x_1} w_1 + f_{x_2} w_2 \right\|^2_{L^2(\Omega)} \ . \tag{2}$$

The minimization problem is ill-posed, which is usually overcome by adding a convex regularization term $\mathcal{R}$ to $\mathcal{S}$. For $\lambda > 0$, the regularized optical flow problem consists in minimization of

$$\boldsymbol{w} \to \frac{1}{\lambda} \mathcal{S}(\boldsymbol{w}) + \mathcal{R}(\boldsymbol{w}) \, . \tag{3}$$

Optical flow methods have been pioneered in [12]. There, the squared L^2-norm of the gradient is used for regularization and therefore the method consists in minimization of

$$\boldsymbol{w} \to \frac{1}{\lambda} \mathcal{S}(\boldsymbol{w}) + \frac{1}{2} \left\| \nabla \boldsymbol{w} \right\|^2_{L^2(\Omega;\mathbb{R}^2)} \ . \tag{4}$$

This regularization approach has the drawback that the computed optical flow field $\boldsymbol{w}$ is not aligned with edges in f_1 and f_2. To overcome this drawback generalized regularization functionals $\mathcal{R}$ have been considered in the literature. See for instance [9, 10, 19, 6], to name but a few. An extensive survey on variational methods in optical flow estimation is given in [18]

Image decomposition models.
Recently, decomposition models of gray-value images into structural and textural components have been studied [14, 16, 15]. Generally speaking, for an image I, these models consist in minimizing the functional

$$(u, v) \mapsto \frac{1}{2\lambda} \left\| u + v - I \right\|^2 + N_U(u) + \gamma N_V(v) \text{ over } u \in U,\, v \in V \tag{5}$$

The minimizer (u, v) of (5) is considered the structural and textural component of I. In [4], various spaces U (such as $BV(\Omega)$, the Sobolev spaces $W_0^{1,p}(\Omega)$, and the homogeneous Besov space $U = \dot{B}^1_{1,1}$) with associated seminorms N_U and duals $V = U^*$, $N_V = (N_U)^*$ have been examined. As it is reported there, the choice $U = BV(\Omega)$ and N_U the total variation seminorm is very interesting, since the dual of the total variation seminorm approximates Meyer's G-norm [14]. The G-norm is suitable to model texture, because it takes small values on oscillating functions.

Optical flow decomposition models.
Quite recently, there have been established decomposition models for optical flow models. In particular, for analyzing experimental fluid flow data, decomposition into solenoidal components (div $\boldsymbol{w}$) and vortices (curl $\boldsymbol{w}$) of the flow $\boldsymbol{w}$ are calculated (see [13, 21, 20]). There, minimizers of functionals of the form

$$\mathcal{S}(\boldsymbol{w}) + \lambda_d \int\limits_{\Omega} |\nabla \text{div } \boldsymbol{w}|^{p_d} dxdy + \lambda_c \int\limits_{\Omega} |\nabla \text{curl } \boldsymbol{w}|^{p_c} dxdy + \gamma \int\limits_{\partial\Omega} (\partial_n \boldsymbol{w})^2 ds \tag{6}$$

with $p_d, p_c \in \{1, 2\}$ are used for optical flow decomposition.
A duality based model for optical flow estimation is proposed in [22]. Functionals of the form

$$E_\theta(\boldsymbol{u}, \boldsymbol{v}) = \int_\Omega \left\{ \sum_d |\nabla u_d| + \frac{1}{2\theta} \sum_d v_d^2 + \lambda \, |\rho(\boldsymbol{u} + \boldsymbol{v})| \right\} dx \tag{7}$$

are minimized. Here, $\boldsymbol{u} = (u_d)_d$ and $\boldsymbol{v} = (v_d)_d$ are flow fields, $|\rho|$ is a data fidelity function, being small if $\boldsymbol{u}+\boldsymbol{v}$ solves the optical flow equation, and $\lambda > 0$, $\theta > 0$ are weighting parameters. The arising optical flow $\boldsymbol{w} = \boldsymbol{u} + \boldsymbol{v}$ is implicitly decomposed into a component $\boldsymbol{u}$ of small total variation and a component $\boldsymbol{v}$ of small L^2-norm.

Outline of the paper.
In this paper we apply the variational decomposition models of [4] to optical flow problems. To do so, we first reformulate the optical flow problem as an image denoising problem for vector valued data (cf. Section 2). In section 3 we recall recent methods for image decomposition of color data [5] and decomposition models for gray valued data [3] and adopt them for optical flow decomposition. We present a general formulation of variational optical flow decomposition which allows for utilizing various spaces and seminorms. In section 4, we particularly focus on the total variation seminorm and Meyer's G-norm. Moreover, a variant of Chambolle's algorithm (originally used for total variation denoising) is used to compute numerical examples in section 5, which demonstrate the feasibility of the proposed method.

2 Reformulation as a Denoising Problem and Optical Flow Decomposition

The matrix $A_0 := \nabla f (\nabla f)^T$ has rank one, is positive semi-definite with non-trivial kernel, which consists of all vector valued functions, which are orthogonal to ∇f. Moreover, $\langle \boldsymbol{u}, \boldsymbol{v} \rangle_{A_0} = \int_\Omega \boldsymbol{u}^T A_0 \boldsymbol{v}$ is an inner product and by $|\boldsymbol{u}|^2_{A_0} := \langle \boldsymbol{u}, \boldsymbol{u} \rangle_{A_0} = \int_\Omega \boldsymbol{u}^T A_0 \boldsymbol{u}$ a seminorm is given. For further rewriting the optical flow least-squares functional $\mathcal{S}$, defined in (2), we use a full rank approximation of A_0, which is derived in two steps. We first regularize A_0 by setting $\tilde{A} := ((A_0)^T A_0 + \epsilon \mathrm{Id})^{\frac{1}{2}}$. Here, Id denotes the identity matrix and $\epsilon > 0$ is a small regularization parameter. This way, $\tilde{A}$ is positive definite. Second, we apply an anisotropic evolution to the matrix $\tilde{A}$ to enhance the structure of the underlying image data. We solve

$$\partial_t a_{ij} = \operatorname{div} g(|\nabla A \nabla A^T|) \nabla a_{ij} \tag{8}$$

$$a_{ij}(0) = \tilde{a}_{ij} \tag{9}$$

It can be checked easily, that the matrix A is positive definite. Moreover, in [7, 17], it is reported that this preprocessing is very appropriate for optical flow

estimation in noisy data. As a consequence, $\langle \boldsymbol{u}, \boldsymbol{v} \rangle_A = \int_\Omega \boldsymbol{u}^T A \boldsymbol{v}$ is a scalar product (which we call A-scalar product) on the weighted L^2-space

$$L^2(\Omega; A) = \left\{ \boldsymbol{u} : \|\boldsymbol{u}\|_A := \sqrt{\langle \boldsymbol{u}, \boldsymbol{u} \rangle_A} < \infty \right\} . \tag{10}$$

The optical flow least squares functional $\mathcal{S}$, defined in (2), can now be approximated by the squared of the A-norm of the optical flow residual. To see this let

$$\hat{\boldsymbol{f}} := \frac{1}{|\nabla f|}(-f_t f_x, -f_t f_y)^T \tag{11}$$

Note that $A_0^{1/2}$, defined by spectral decomposition, equals $\frac{1}{|\nabla f|} A_0$. Then,

$$\begin{aligned}
&\left\| A_0^{1/2} \cdot \boldsymbol{w} - \hat{\boldsymbol{f}} \right\|^2_{L^2(\Omega;\mathbb{R}^2)} \\
&= \int_\Omega [(A_0^{1/2} \cdot \boldsymbol{w})_1 - \hat{\boldsymbol{f}}_1]^2 + [(A_0^{1/2} \cdot \boldsymbol{w})_2 - \hat{\boldsymbol{f}}_2]^2 \\
&= \int_\Omega \left[\frac{f_x^2 w_1 + f_x f_y w_2}{|\nabla f|} + \frac{f_x f_t}{|\nabla f|} \right]^2 + \left[\frac{f_x f_y w_1 + f_y^2 w_2}{|\nabla f|} + \frac{f_y f_t}{|\nabla f|} \right]^2 \\
&= \int_\Omega \frac{f_x^2 + f_y^2}{|\nabla f|^2} (f_x w_1 + f_y w_2 + f_t)^2 \\
&= \|\nabla f \cdot \boldsymbol{w} + f_t\|^2_{L^2(\Omega)} ,
\end{aligned} \tag{12}$$

Using the notation

$$\tilde{\boldsymbol{f}} = A^{-\frac{1}{2}} \hat{\boldsymbol{f}} , \tag{13}$$

we find that

$$\|\nabla f \cdot \boldsymbol{w} + f_t\|_{L^2(\Omega)} = \left\| A_0^{1/2} \cdot \boldsymbol{w} - \hat{\boldsymbol{f}} \right\|_{L^2(\Omega;\mathbb{R}^2)} \approx \left\| \boldsymbol{w} - \tilde{\boldsymbol{f}} \right\|_A . \tag{14}$$

This relation shows that the optical flow least squares functional $\mathcal{S}$ defined in (2) can be approximated, and in fact replaced, by the squared norm of the weighted L^2-space defined in (10).

3 Decomposition Models for Optical Flow

From now on, taking into account (14), we regard the optical flow problem as an imaging problem. The actual difference to standard image decomposition [3] is that here the function to be filtered, $\tilde{\boldsymbol{f}}$, is vector valued and that weighted norms are used in the fit-to-data functional.

Inspired by the work on variational decomposition of color data in [5] we consider minimizing

$$\mathcal{L}(\boldsymbol{u}, \boldsymbol{v}) := \frac{1}{2\lambda} \left\| (\boldsymbol{u} + \boldsymbol{v}) - \tilde{\boldsymbol{f}} \right\|^2_A + N_U(\boldsymbol{u}) + \gamma N_V(\boldsymbol{v}) ; \tag{15}$$

over $\boldsymbol{u} \in U$ and $\boldsymbol{v} \in V$. Thus, optical flow $\boldsymbol{w}$ is decomposed into $\boldsymbol{w} = \boldsymbol{u} + \boldsymbol{v}$. Several spaces and seminorms can be considered for U, V, N_U, N_V to model structure and texture component of optical flow, compare [4].

Total variation model.
Here, we take $U = \mathrm{BV}(\Omega, \mathbb{R}^2)$, which is defined as the space of functions $\boldsymbol{f} \in L^\infty(\Omega, \mathbb{R}^2)$, with the property

$$J(\boldsymbol{f}) := \sup \left\{ \int_\Omega \boldsymbol{f} \cdot \mathrm{div}(\boldsymbol{p}) \ : \ \boldsymbol{p} \in C_c^1(\Omega, \mathbb{R}^2 \times \mathbb{R}^2), \ \|\boldsymbol{p}\|_{L^\infty(\Omega, \mathbb{R}^2 \times \mathbb{R}^2)} \leq 1 \right\} < \infty \,, \tag{16}$$

where $C_c^1(\Omega, \mathbb{R}^2 \times \mathbb{R}^2)$ is the space of differentiable functions with compact support in Ω; moreover, $\|\boldsymbol{p}\|_{L^\infty(\Omega, \mathbb{R}^2 \times \mathbb{R}^2)}$ is the L^∞-norm of the Frobenius-norm of $\boldsymbol{p}$.

We take $J(\boldsymbol{f})$, which is called total variation seminorm of $\boldsymbol{f}$, as N_U. The space V consists of $\mathbb{R}^2$- valued distributions $\boldsymbol{g}$, which can be written as $\boldsymbol{g} = \mathrm{div}(\boldsymbol{p})$, with $\boldsymbol{p} \in L^\infty(\Omega, \mathbb{R}^2 \times \mathbb{R}^2)$. The divergence operator is a distributional derivative here. On V we use for N_V the G-norm [14], which is defined as

$$\|\boldsymbol{g}\|_G := \inf\{\|\boldsymbol{p}\|_{L^\infty(\Omega, \mathbb{R}^2 \times \mathbb{R}^2)} \ : \ \boldsymbol{p} \in L^\infty(\Omega, \mathbb{R}^2 \times \mathbb{R}^2), \boldsymbol{g} = \mathrm{div}(\boldsymbol{p})\} \tag{17}$$

The G-norm is suitable to model texture, because it takes small values on oscillating functions.

Sobolev space model.
In this model, we choose U as the Sobolev space $W_0^{1,p}(\Omega, \mathbb{R}^2)$ and N_U as the standard Sobolev seminorm (see [2] for a reference of general Sobolev spaces). Moreover, we use for V the dual space of U, which is $V = W^{-1,q}(\Omega, \mathbb{R}^2)$, where q is the conjugate of p, and N_V is the corresponding Sobolev-Norm.

Besov space model.
Here $U = \dot{B}^1_{1,1}(\Omega, \mathbb{R}^2)$ is the homogenous Besov space with norm N_U (see also [2]) and V is its dual $\dot{B}^\infty_{-1,\infty}(\Omega, \mathbb{R}^2)$

For gray valued images, as stated in [4], the total variation model gives the most meaningful decomposition results of the three mentioned above. This is why we concentrate on this case in detail and apply it for the decomposition of optical flow.

4 Numerical Implementation

In the following section, we discretize the total variation model and derive numerical algorithms for its minimization. From now on we only consider a discrete and finite-dimensional setting.

Discrete one-channel images are matrices $U = (u_{i,j})$ of size $M \times N$, representing continuous images on Ω. Analogously, multi-channel images are matrices of size $M \times N$ with vectorial entries $\boldsymbol{u}_{i,j} = (u^1_{i,j}, u^2_{i,j})^T$. We denote by $X := (\mathbb{R}^2)^{M\times N}$ the space of multi-channel matrices.

For a discrete matrix $H = (h_{ij})$ we define the discrete gradient $\nabla H = (\nabla_x H, \nabla_y H)^T$ as

$$\nabla_x h_{i,j} := \begin{cases} h_{i+1,j} - h_{i,j} & \text{if } i < M \\ 0 & \text{if } i = M \end{cases} \tag{18}$$

and

$$\nabla_y h_{i,j} := \begin{cases} h_{i,j+1} - h_{i,j} & \text{if } j < N \\ 0 & \text{if } j = N \end{cases} . \tag{19}$$

The discrete total variation of a vector field $\boldsymbol{u}$ is defined by

$$J(\boldsymbol{u}) = \sum_{i,j} \sqrt{(\nabla_x u^1_{i,j})^2 + (\nabla_y u^1_{i,j})^2 + (\nabla_x u^2_{i,j})^2 + (\nabla_y u^2_{i,j})^2}. \tag{20}$$

Moreover, the discrete divergence operator of the tensor $\boldsymbol{u}$ is defined by

$$[\mathrm{div}(\boldsymbol{u})]_{i,j} = \begin{cases} u^1_{i,j} - u^1_{i-1,j} & \text{if } 1 < i < M \\ u^1_{i,j} & \text{if } i = 1 \\ -u^1_{i-1,j} & \text{if } i = M \end{cases} + \begin{cases} u^2_{i,j} - u^2_{i,j-1} & \text{if } 1 < j < N \\ u^2_{i,j} & \text{if } j = 1 \\ -u^2_{i-1,j} & \text{if } j = N \end{cases} .$$

The discrete divergence operator, as in the continuous setting again denoted by div, of $\boldsymbol{u}$ is defined as the discrete divergences of the components. For definition of the discrete time derivative, we fix a small constant $\delta t > 0$. Given two subsequent frames U_k, $U_{k+1} \in \mathbb{R}^{M\times N}$ of discrete one-channel images, we define

$$\nabla_t U = \frac{U_{k+1} - U_k}{\delta t}. \tag{21}$$

The discrete formulas in (18), (19) and (21) give approximations of $\tilde{\boldsymbol{f}}$ as defined in (13) and hence also of A_0 and its regularization A. The A-scalar product in $L^2(\Omega; A)$ as defined in (10) is then approximated by

$$\langle \boldsymbol{u}, \boldsymbol{v} \rangle_X = \sum_{i,j} \boldsymbol{u}^T_{i,j} A_{i,j} \boldsymbol{v}_{i,j} \,, \tag{22}$$

where $A_{i,j} \in \mathbb{R}^{2\times 2}$.

Approximation of the discrete G-Norm by the dual J^* of J.
For definition of the G-norm, we set

$$K = \{v \in X \ : \ \text{there exists } \boldsymbol{p} = (p_1, p_2) \in X \times X \text{ such that } v = \mathrm{div}(\boldsymbol{p})\} \tag{23}$$

For $v \in K$, the discrete G-norm $\|\cdot\|$ is then given by

$$\|v\|_G = \inf \{\|\boldsymbol{p}\|_\infty : \boldsymbol{p} \in X \times X, v = \operatorname{div}(\boldsymbol{p})\}. \tag{24}$$

Here $\|\boldsymbol{p}\|_\infty$ denotes the l^∞-norm of the Frobenius-norm of the matrix $\boldsymbol{p}$. This definition of the discrete G-norm is difficult to implement numerically. For numerical purposes it is convenient, as proposed in [4], to use the Fenchel dual

$$J^*(v) := \sup\{\langle v, u\rangle - J(u) : (u, v) \in X \times X\} \tag{25}$$

of J. Since J is a seminorm, an elementary calculation shows that there exists a convex, closed set $K_1 \subseteq X$ such that

$$J^*(v) = \begin{cases} \infty & \text{if } v \in K_1 \\ 0 & \text{otherwise} \end{cases}. \tag{26}$$

Similar to [4], one can show that K_1 in (26) is given by

$$K_1 = \{\operatorname{div}(\boldsymbol{p}) : \boldsymbol{p} \in X \times X \text{ and } \|\boldsymbol{p}\|_\infty \leq 1\} \tag{27}$$

Because of this characterization, J^* is much easier to compute than the G-norm. The close relationship between G-norm and J^* is revealed by the following theorem:

Theorem 1. *Let α, λ, $\gamma > 0$. Consider the following minimization problems over $X \times X$:*

(A) $\min_{\boldsymbol{u}+\boldsymbol{v}=\tilde{\boldsymbol{f}}} J(\boldsymbol{u}) + \alpha \|\boldsymbol{v}\|_G$
(B) $\min_{\boldsymbol{u}+\boldsymbol{v}=\tilde{\boldsymbol{f}}} J(\boldsymbol{u}) + J^*(\frac{\boldsymbol{v}}{\gamma})$
(C)

$$\min_{(\boldsymbol{u},\boldsymbol{v})} H_{\lambda,\gamma}(\boldsymbol{u}, \boldsymbol{v}) := \frac{1}{2\lambda} \left\| \boldsymbol{u} + \boldsymbol{v} - \tilde{\boldsymbol{f}} \right\|_X^2 + J(\boldsymbol{u}) + J^*(\frac{\boldsymbol{v}}{\gamma}) \tag{28}$$

Then minimizers for all three problems exist, and for (C) it is unique. Moreover, there exists a relation between α and γ, such that a minimizer of (A) is a minimizer of (B) and vice versa. Moreover, as $\lambda \downarrow 0$, the minimizers of (C) converge to a minimizer of (B).

Proof. Here, we only prove existence and uniqueness of a minimizer of (C), following the proof in [3] for gray valued images. The other statements can then be proven analogously and are therefore omitted.

Existence of a minimizer of $H_{\lambda,\gamma}$: The set $X \times \gamma K$ is closed in the finite dimensional space $X \times X$ and the restriction of $H_{\lambda,\gamma}$ to $X \times \gamma K$ is continuous. Therefore lower semicontinuity of $H_{\gamma,\lambda}$ holds, that is, for every sequence $(\boldsymbol{u}_k, \boldsymbol{v}_k) \in X \times X$

$$H_{\gamma,\lambda}(\boldsymbol{u}, \boldsymbol{v}) \leq \liminf_{(\boldsymbol{u}_k,\boldsymbol{v}_k)\to(\boldsymbol{u},\boldsymbol{v})} H_{\gamma,\lambda}(\boldsymbol{u}_k, \boldsymbol{v}_k).$$

Next we show coercivity for $H_{\lambda,\gamma}$ on $X \times X$, i.e. we prove that

$$H_{\lambda,\gamma}(\boldsymbol{u},\boldsymbol{v}) \to \infty \text{ if } \|(\boldsymbol{u},\boldsymbol{v})\|_{X\times X} \to \infty \,.$$

Let $(\boldsymbol{u},\boldsymbol{v}) \in X \times \gamma K$. By the definition of γK there exists $\boldsymbol{p} \in X \times X$ such that $\operatorname{div}(\boldsymbol{p}) = \boldsymbol{v}$ and $\|\boldsymbol{p}\|_\infty \leq \gamma$. Therefore we have

$$\|\boldsymbol{v}\|_X^2 = \sum_{i,j} \operatorname{div}(\boldsymbol{p})_{i,j}^T A_{i,j} \operatorname{div}(\boldsymbol{p})_{i,j} \,,$$

Since $\boldsymbol{p}$ is uniformly bounded with respect to $\boldsymbol{v}$, we see that $\|\cdot\|_X$ is bounded on γK. Therefore, if $\|(\boldsymbol{u},\boldsymbol{v})\|_{X\times X} \to \infty$ with $\boldsymbol{v} \in \gamma K$, it follows that $\|\boldsymbol{u}\|_X \to \infty$, hence $H_{\lambda,\gamma}(\boldsymbol{u},\boldsymbol{v}) \geq \left\|\boldsymbol{u}+\boldsymbol{v}-\tilde{\boldsymbol{f}}\right\|_X \to \infty$, which gives coercivity. In summary, since $H_{\lambda,\gamma}$ is lower semi-continuous and coercive in $X \times X$, a minimizer for (15) exists.

Uniqueness of a minimizer of $H_{\lambda,\gamma}$: The functional $H_{\lambda,\gamma}(\boldsymbol{u},\boldsymbol{v})$ is strictly convex on $X \times \gamma K$ up to direction $(\boldsymbol{u},-\boldsymbol{u})$. So it might happen for some $t > 0$, that both $(\boldsymbol{u},\boldsymbol{v})$ and $(\boldsymbol{u}+t\boldsymbol{u},\boldsymbol{v}-t\boldsymbol{u})$ are (global) minimizers of (15). We show that in this case, $\boldsymbol{u} = 0$, which means that the two minimizers coincide. Indeed, from $H_{\lambda,\gamma}(\boldsymbol{u}+t\boldsymbol{u},\boldsymbol{v}-t\boldsymbol{u}) = H_{\lambda,\gamma}(\boldsymbol{u},\boldsymbol{v}) + tJ(\boldsymbol{u})$ and the assumption that both are global minimizers, we conclude that $J(\boldsymbol{u}) = 0$. From the definition of the discrete total variation it follows that $\boldsymbol{u}$ is a constant. Moreover, since $\boldsymbol{u} \in \gamma K$, there exists $\boldsymbol{p} \in X \times X$ such that $\boldsymbol{u} = \operatorname{div}(\boldsymbol{p})$. Therefore

$$\sum_{i,j} \boldsymbol{u}_{i,j} = \sum_{i,j} \operatorname{div}(\boldsymbol{p})_{i,j} = 0.$$

The last equality holds, since each summand occurs exactly four times in $\sum_{i,j} \operatorname{div}(\boldsymbol{p})_{i,j}$, twice with a plus, twice with a minus sign.

Theorem (1) enables us to discretize the G-norm in functional(15) by J^* and minimize $H_{\lambda,\gamma}$ numerically. Using Equation (26), $H_{\lambda,\gamma}(\boldsymbol{u},\boldsymbol{v})$ can be expressed in the more convenient form

$$H_{\lambda,\gamma}(\boldsymbol{u},\boldsymbol{v}) = \begin{cases} \frac{1}{2\lambda}\left\|\boldsymbol{u}+\boldsymbol{v}-\tilde{\boldsymbol{f}}\right\|_X^2 + J(\boldsymbol{u}) & \text{if } \boldsymbol{v} \in \gamma K_1 \\ \infty & \text{otherwise} \end{cases} . \tag{29}$$

In the following we investigate an *alternating direction* algorithm for minimization of $H_{\lambda,\gamma}$. It consists of the following two steps:

1. Choose $\boldsymbol{v}^{(0)} \in \gamma K_1$
2. For $k = 0, 1, 2, \ldots$
   - Calculate a minimizer $\boldsymbol{u}^{(k)} \in \gamma K$ of

$$\frac{1}{2\lambda}\left\|\boldsymbol{u}+\boldsymbol{v}^{(k)}-\tilde{\boldsymbol{f}}\right\|_X^2 + J(u) \,. \tag{30}$$

– Calculate a minimizer $\boldsymbol{v}^{(k+1)}$ of

$$\left\|\boldsymbol{u}^{(k)} + \boldsymbol{v} - \tilde{\boldsymbol{f}}\right\|_X^2 . \tag{31}$$

– Continue

We state convergence of the iteration process. The proof is omitted here, since it is again along the lines in [3].

Theorem 2. *The sequence* $(\boldsymbol{u}^{(k)}, \boldsymbol{v}^{(k)})$ *converges to the unique solution* $(\hat{\boldsymbol{u}}, \hat{\boldsymbol{v}})$ *of* (28).

We stress that $\tilde{\boldsymbol{v}}$ solves (31) if and only if $\tilde{\boldsymbol{w}} = \tilde{\boldsymbol{f}} - \boldsymbol{u} - \tilde{\boldsymbol{v}}$ is a minimizer of the functional

$$\boldsymbol{w} \to \frac{1}{2\gamma}\left\|\boldsymbol{u} + \boldsymbol{w} - \tilde{\boldsymbol{f}}\right\|_X^2 + J(\boldsymbol{w}) . \tag{32}$$

This formulation actually shows that also minimization with respect to $\boldsymbol{v}$ can be realized by total variation denoising. Therefore both iteration steps of the alternating direction algorithm can be realized by total variation denoising, which can be implemented with a variant of Chambolle's projection algorithm [8]. Therefore, in the sequel, we only consider total variation denoising for vector valued data $\boldsymbol{u}^\delta$, which consists in minimization of

$$\frac{1}{2\lambda}\left\|\boldsymbol{u} - \boldsymbol{u}^\delta\right\|_X^2 + J(\boldsymbol{u}) . \tag{33}$$

Following Chambolle's algorithm [8], we derive an iterative procedure for minimizing (33).

Let

$$\boldsymbol{p}(0) := (\boldsymbol{p}^1(0), \boldsymbol{p}^2(0)) := \begin{pmatrix} p^{1,1}(0)\, p^{1,2}(0) \\ p^{2,1}(0)\, p^{2,2}(0) \end{pmatrix} = 0 .$$

For $k = 0, 1, 2, \ldots$ set

$$\boldsymbol{q}(k) = \left[\operatorname{div}(\boldsymbol{p}(k)) - \boldsymbol{u}^\delta/\lambda\right]$$

Each entry $A_{i,j}$ of the matrix A is a 2×2-matrix, which is positive definite. We set

$$S_{i,j} := A_{i,j}^{1/2} ,$$

the root of A. Then componentwise

$$\boldsymbol{p}^1(k+1) = \frac{\boldsymbol{p}^1(k) + \tau\left[\nabla\left(S_{1,1}\boldsymbol{q}^1(k) + S_{1,2}\boldsymbol{q}^2(k)\right)\right]}{1 + \tau\left|\nabla\left(S_{1,1}\boldsymbol{q}^1(k) + S_{1,2}\boldsymbol{q}^2(k) + S_{2,1}\boldsymbol{q}^1(k) + S_{2,2}\boldsymbol{q}^2(k)\right)\right|} \tag{34}$$

and

$$\boldsymbol{p}^2(k+1) = \frac{\boldsymbol{p}^2(k) + \tau\left[\nabla\left(S_{2,1}\boldsymbol{q}^1(k) + S_{2,2}\boldsymbol{q}^2(k)\right)\right]}{1 + \tau\left|\nabla\left(S_{1,1}\boldsymbol{q}^1(k) + S_{1,2}\boldsymbol{q}^2(k) + S_{2,1}\boldsymbol{q}^1(k) + S_{2,2}\boldsymbol{q}^2(k)\right)\right|}. \tag{35}$$

Theorem 3. *Let $\pi_{\lambda K}$ the orthogonal projector onto λK, where K is as in* (23)*. If τ, as in* (34) *and* (35)*, is chosen sufficiently small, then div $\boldsymbol{p}(k)$ converges to $\pi_{\lambda K}(\boldsymbol{u}^\delta)$. The solution of* (33) *is given by*

$$\boldsymbol{u} = \boldsymbol{u}^\delta - \pi_{\lambda K}(\boldsymbol{u}^\delta) \; . \tag{36}$$

Proof. The proof is along the lines of [8] and thus it is omitted here.

From Theorem 3 it follows that the minimizer u_α of (33) satisfies

$$u_\alpha = \boldsymbol{u}^\delta - \lambda \lim_{k\to\infty} \operatorname{div} \boldsymbol{p}(k) \; .$$

This theorem completes the numerical analysis of the functional $H_{\lambda,\gamma}$.

5 Results

We performed numerical experiments on several image sequences, which are publicly available at [1]. We decomposed the optical flow in the *rubber whale* sequence (see Figure 1). The curtain and the two round pieces at the bottom move to the left, while the other pieces move to the right, see (a). The moving large structures, such as the fence and the two round objects, are captured in the cartoon component (b), while for instance the curtain contains texture movement in (d). In order to improve visibility, the (scaled) magnitude of the flow u and v is shown in (c) and (e), respectively. The whole optical flow field is shown in (f) and (g). In the *Mini Cooper* sequence shown in Figure 2, a man is closing the trunk of a car (a). The cartoon part u of the optical flow consists of the moving tailgate and the man (b). The magnitude of flow u is shown in (c). The slight motion of the trees in the background is completely contained in the texture component v of the optical flow, shown in (d). The (upscaled) magnitude of v is given in (e).
These two examples show the advantages of our method quite well, separating different kinds of movements in an image sequence.
In the Dimetrodon sequence shown in Figure 3, we examine directions of the computed flow field and its decomposition in greater detail. The main direction of movement of the head can be seen in flow field u in (c), where neighboring flow vectors are often parallel. Oscillating patterns are captured in v shown in (d), where the directions of the flow vectors can differ very much between neighboring pixels.

6 Conclusion

We presented a general approach for decomposition of the optical flow of an image sequence into structural and textural components. A variational framework has been established, which allows to use various functionals for different kinds of texture extraction. Numerical examples demonstrate the effectivity of total variation norm, respectively G-norm, decomposition. In the future, we plan to study other possible seminorms in (15) as well and plan to compare the outcome of the different methods.

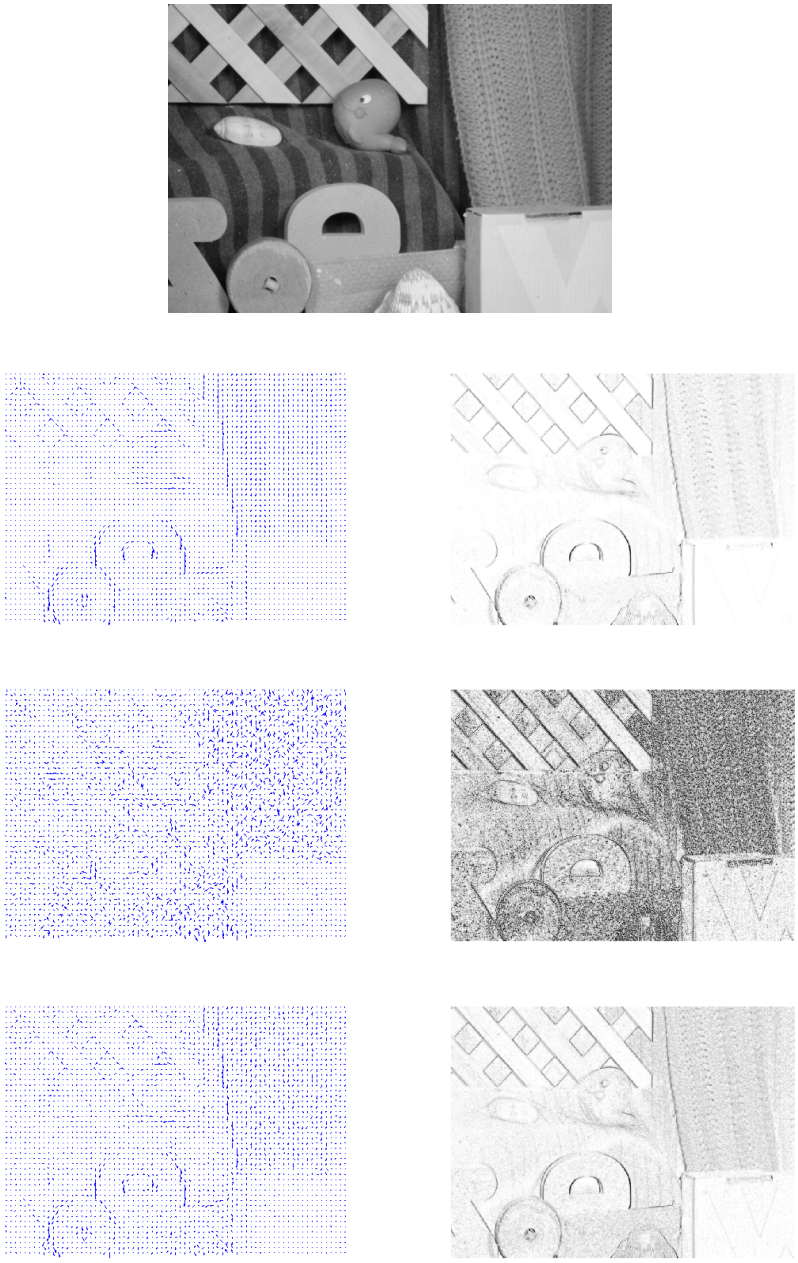

Fig. 1. (a) On top: Frame 10 of the rubber whale sequence (584 × 388 pixels). (b) Top left: Cartoon part u of the flow between frame 10 and frame 11. (c) Top right: Norm of cartoon part u. (d) Middle left: Texture part v. (e) Middle right: Norm of texture part v. (f) Bottom left: The flow field $w = u + v$. (g) Bottom right: Norm of the flow field $w = u + v$.

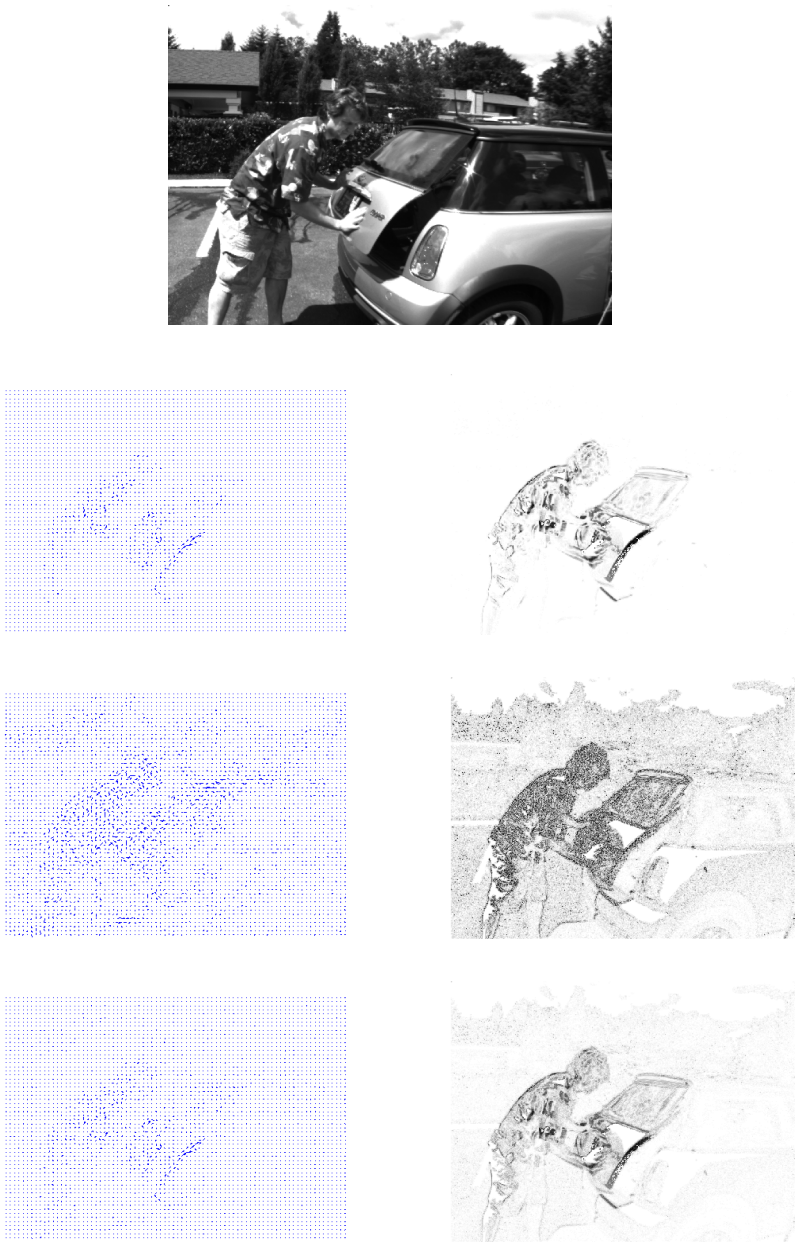

Fig. 2. (a) On top: Frame 10 of the Mini Cooper sequence (640 × 480 pixels). (b) Top left: Cartoon part u of the flow between frame 10 and frame 11. (c) Top right: Norm of cartoon part u. (d) Middle left: Texture part v. (e) Middle right: Norm of texture part v. (f) Bottom left: The flow field $w = u + v$. (g) Bottom right: Norm of the flow field $w = u + v$.

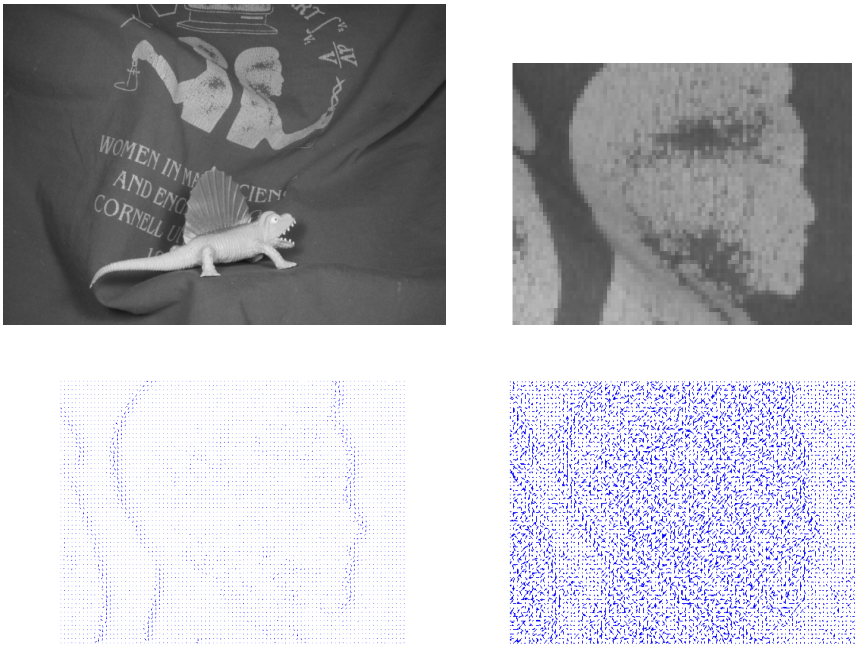

Fig. 3. (a) Top left: Frame 10 of the dimetrodon sequence (584 × 388 pixels). (b) Top right: A detailed view of the head in the upper middle of (a). (c) Bottom left: Detailed view of cartoon part u of the flow field between frame 10 and frame 11. (d) Bottom right: Detailed view of texture part v.

Acknowledgement

This work has been supported by the Austrian Science Fund (FWF) within the national research networks Industrial Geometry, project 9203-N12, and Photoacoustic Imaging in Biology and Medicine, project S10505-N20. The research stay of Dr. Zakaria Belhachmi in Innsbruck has been funded by the "'Frankreich Schwerpunkt"' of the University of Innsbruck. The work of the first author has been partly supported by the Austrian Ministry for Economy and Labour and by the Government of Upper Austria within the framework "Industrial Competence Centers".
We also want to thank the referees for their useful comments.

References

1. http://vision.middlebury.edu/flow/.
2. H. Amann. Compact embeddings of sobolev and besov spaces. *Glasnik Matematicki*, 35(55):161–177, 2000.

3. J.-F. Aujol, G. Aubert, L. Blanc-Feraud, and A. Chambolle. Image decomposition into a bounded variation component and an oscillating component. *Journal of Mathematical Imaging and Vision*, 22(1):71–88, 2005.
4. J.-F. Aujol and A. Chambolle. Dual norms and image decomposition models. *International Journal of Computer Vision*, 63(1):85–104, 2005.
5. J.-F. Aujol and S.-H. Kang. Color image decomposition and restoration. *Journal of Visual Communication and Image Representation*, 17(4):916–928, 2006.
6. T. Brox, A. Bruhn, N. Papenberg, and J. Weickert. High accuracy optical flow estimation based on a theory for warping. In *European Conference on Computer Vision*, pages 25–36, 2004.
7. A. Bruhn. *Variational optic flow computation: Accurate modeling and efficient numerics*. PhD thesis, Saarland University, Germany, 2006.
8. A. Chambolle. An algorithm for total variation minimization and applications. *Journal of Mathematical Imaging and Vision*, 20(1–2):89–97, 2004.
9. I. Cohen. Nonlinear variational method for optical flow computation. In *Proc. Eigth Scandinavian Conference on Image Analysis*, volume 1, pages 523–530, May 1993. Tromso, Norway.
10. R. Deriche, P. Kornprobst, and G. Aubert. Optical flow estimation while preserving its discontinuities. In *Proc. Second Asian Conference on Computer Vision*, volume 2, pages 290–295, Dec. 1995. Singapore.
11. D.J. Fleet and Y. Weiss. *Optical Flow Estimation*, chapter 15, pages 239–258. Mathematical Models of Computer Vision: The Handbook. Springer, 2005.
12. B.K.P. Horn and Schunck B.G. Determining optical flow. *Artificial Intelligence*, 17:185–203, 2004.
13. E. Kohlberger, T.and Memin and C. Schnoerr. Variational dense motion estimation using helmholtz decomposition. In *Scale Space Methods in Computer Vision*, volume 2695, pages 432–448, Dec. 2003. Springer LNCS.
14. Y. Meyer. Oscillating patterns in image processing and in some nonlinear evolution equations. In *The Fifteenth Dean Jaqueline B. Lewis Memorial Lectures*, March 2001.
15. J.L. Starck, M. Elad, and D.L. Donoho. Image decomposition via the combination of sparse representations and a variational approach. *IEEE Transactions on Image Processing*, 14(10):1570–1582, 2005.
16. L.A. Vese and S. Osher. Modeling textures with total variation minimization and oscillating patterns in image processing. *Journal of Scientific Computing*, 19:553–572, 2003.
17. J. Weickert, A. Bruhn, T. Brox, and N. Papenberg. *A Survey on Variational Optic Flow Methods for Small Displacements*, chapter 1, pages 103–136. Mathematical Models for Registration and Applications to Medical Imaging. Springer, 2006.
18. J. Weickert and C. Schnoerr. A theoretical framework for convex regularizers in pde-based computation of image motion. *International Journal of Computer Vision*, 45(3):245–264, 2001.
19. J. Weickert and C. Schnoerr. Variational optic flow computation with a spatio-temporal smoothness constraint. *Journal of Mathematical Imaging and Vision*, 14(3):245–255, 2001.
20. J. Yuan, C. Schnoerr, and G. Steidl. Simultaneous higher-order optical flow estimation and decomposition. *SIAM J. Scientfic Computing*, 29(6):2283–2304, 2007.
21. J. Yuan, C. Schnoerr, G. Steidl, and Becker F. A study of non-smooth convex flow decomposition. In *Proc. Variational Methods, Geometris and Level Set Methods in Computer Vision*, volume 3752, pages 1–12, 2005. Springer.
22. C. Zach, T. Pock, and H. Bischof. A duality based approach for realtime TV $-$ L1 optical flow. In *DAGM*, 2007.